RSC Advances

ROYAL SOCIETY OF CHEMISTRY

www.rsc.org/advances

P-type Mg doped $CuAlO_2$ films with high crystallinity are prepared by pulsed laser deposition followed by annealing, and exhibit enhanced conductivity and tunable optical band gap.

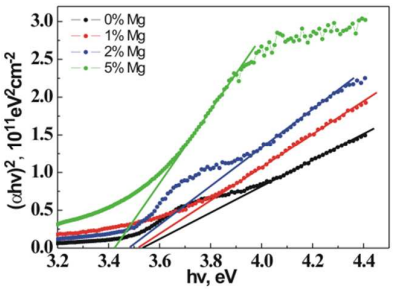

Structural, electrical and optical properties of Mg-doped $CuAlO_2$ films by pulsed laser deposition

Y.S. Zou*, H.P. Wang, S.L. Zhang, D. Lou, Y.H. Dong, X.F. Song, H.B. Zeng*

School of Materials Science and Engineering, Institute of Optoelectronics & Nanomaterials, Nanjing University of Science and Technology, Nanjing, Jiangsu, 210094, China

* Corresponding author. Fax: +86 25 84303279, Email: yshzou75@gmail.com, zeng.haibo @njust.edu.cn

Abstract

The $CuAl_{1-x}Mg_xO_2$ (x=0, 0.01, 0.02, 0.05) films were deposited on sapphire and fused silica substrates by pulsed laser deposition and underwent annealing in Ar ambient at the temperature of 1000 ℃. The effect of Mg concentrations on the structural, morphological, electrical and optical properties was investigated by X-ray diffraction (XRD), X-ray photoelectron spectroscopy (XPS), scanning electron microscope (SEM), UV-visible-NIR spectrophotometer and Hall effect measurement system. The results indicate that Mg is successfully doped into $CuAlO_2$ film with p-type conduction after annealing. Single and pure-phase $CuAl_{1-x}Mg_xO_2$ (x=0, 0.01, 0.02, 0.05) films with c-axis orientation are obtained on sapphire substrates in the studied doping range, and secondary phase is not detected by XRD measurements. The substitution of Mg^{2+} ions in Al^{3+} sites induces lattice distortion and results in the decline of the crystalline quality. The Hall effect measurement reveals that the carrier concentration increases and Hall mobility decreases with the increase of Mg doping concentration. The resistivity of the $CuAl_{1-x}Mg_xO_2$ films decreases and then increases with increasing Mg doping concentration from 0 to 5%. The minimum resistivity of 11.45 Ω·cm is obtained at room temperature for the $CuAl_{1-x}Mg_xO_2$ films with x=2%. The optical transmittance gradually reduces with the increase of Mg concentration due to the enhancement of absorption of incident photons. The optical band gaps of $CuAl_{1-x}Mg_xO_2$ films are found to decrease from 3.54 to 3.43 eV as the Mg doping concentration from 0 to 5% due to the formation of impurity energy levels.

Keywords: Oxide materials, Thin films, Microstructure, Electrical properties, Optical properties

1. Introduction

As a promising material attracting much attention, both of n-type and p-type transparent conducting oxides (TCOs) have been used as transparent electrodes for electronics technology, such as solar cells [1], transistors [2], photodetectors [3], and light-emitting diodes [4, 5] owing to their functional combination of transparency and electrical conductivity. However, most of the known TCOs are n-type semiconductor materials [6-8], such as tin oxide, zinc oxide, indium oxide and cadmium oxide, no p-type TCOs were found until the report of the delafossite-type $CuAlO_2$ fabricated by Kawazoe[9] using pulsed laser deposition method in 1997. Many efforts have been devoted so far to fabricate p-type $CuAlO_2$ and numerous studies on the improvement of optical and electrical properties of the deposited $CuAlO_2$ films have been carried out [10-14]. Unfortunately, some difficulties, including high crystallization temperature, introduction of secondary phase and low conductivity were encountered for the deposited $CuAlO_2$ films [15, 16]. Post-annealing treatment in N_2 or Ar atmosphere as an important and very effective technique has been employed to yield the crystalline $CuAlO_2$ film and improve the structural properties. Lan et al found that the crystallinity of $CuAlO_2$ films deposited by magnetron sputtering was improved with increasing the annealing temperature in N_2 ambient, and the annealed film showed the preferred c-axis orientation [17]. Compared to n-type TCOs, both conductivity and transparency of the reported p-type TCOs are still much inferior, especially for the conductivity of $CuAlO_2$ film which is three or four orders of magnitude lower than that of popular n-type TCOs, which have limited the applications of $CuAlO_2$ films in photovoltaic cells, gas sensors, light-emitting diodes and transistors. Therefore, improving the electrical property of $CuAlO_2$ film and manufacturing of pure-phase $CuAlO_2$ film seem to be necessary for practical applications and are an important issue.

$CuAlO_2$ with a wide direct band gap of 3.5 eV at room temperature has an ABO_2 delafossite structure. Therefore, the substitution of bivalent cations in B sites is generally considered as a

direct and effective route to increasing electrical conductivity. Recently, considerable efforts have been made to improve the properties of Cu-based delafossites by using the doping technology, such as Mg/Mn/Ca/Zn-doped $CuAlO_2$/$CuScO_2$/$CuCrO_2$/$CuYO_2$ [18-21]. Nagarajan et al reported the Mg-doped $CuCrO_2$ film prepared by RF sputtering with a conductivity of 220 S cm^{-1} and found that the optimal value for doping was 5 at.% [18]. However, the optical transmittance in the visible region of $CuCr_{1-x}Mg_xO_2$ film is in the range of only 30-40%. Zhu et al found that substituting Al^{3+} in the $CuAlO_2$ film deposited by chemical solution method with Mg^{2+} increases the transmittance in the visible region and electrical conductivity. The conductivity of the 1 at.% Mg-doped $CuAlO_2$ film is up to 5.2×10^{-3} S/cm at 300 K [22]. Dong et al reported that the conductivity of the $CuAlO_2$ film deposited by RF magnetron sputtering exhibited notable improvement through Mg doping, and the conductivity of the $CuAl_{0.98}Mg_{0.02}O_2$ film is three orders of magnitude higher than that of undoped $CuAlO_2$ film [23].

So far, several growth methods, such as pulsed laser deposition (PLD) [9, 24], chemical vapor deposition (PECVD) [25], electron beam evaporation [26] magnetron sputtering [17, 27-29], sol-gel [30] and spraypyrolysis [31], have been applied to grow $CuAlO_2$ films. Among those methods, pulsed laser deposition technique has been considered largely for the growth of device quality films and is promising in preparing $CuAlO_2$ films over the traditional deposition methods due to its several advantages, including good adhesion to the substrate, reproducibility and controllability of stoichiometry and crystal structure, and the easy deposition of alloys and compounds of materials with different vapor pressures. Therefore, PLD is beneficial to the deposition of $CuAlO_2$ film. However, the effect of Mg content on the properties of $CuAlO_2$ films deposited by PLD is less studied. In this study, Mg-doped $CuAlO_2$ films were deposited on sapphire substrates by PLD. Then, the deposited films were conducted the annealing treatment in Ar ambient to improve the phase purity and crystallinity. The influence of Mg substitution on the structural, electrical and optical properties of Mg-doped $CuAlO_2$ films is systematically

investigated.

2. Experimental

Polycrystalline targets of $CuAl_{1-x}Mg_xO_2$ (x=0, 0.01, 0.02, 0.05) were prepared by a conventional solid-state reaction. Stoichiometric amounts of high purity Cu_2O, Al_2O_3 and MgO were carefully mixed. Then the reactants were calcined at 1150 ℃ for 10 hours to generate $CuAl_{1-x}Mg_xO_2$ (x=0, 0.01, 0.02, 0.05) powders. After ball milling for 6 hours, the calcined powders were pressed into disk as the target, and sintered at 1150 ℃ for 4 hours. Then the ceramic targets for PLD were obtained.

The Mg-doped $CuAlO_2$ films were grown on (0001) sapphire and fused silica by PLD using the calcined disk target. The substrates were cleaned sequentially with acetone, ethanol, and deionized water in an ultrasonic cleaner. The distance between substrate and target was 60 mm. Prior to deposition, the chamber was pumped down to 10^{-3} Pa by rotary pump and molecular pump. The target rotated continuously at 10 rpm was ablated with KrF excimer laser at laser energy of 230 mJ and frequency of 5 Hz. The high-purity oxygen was introduced into the chamber to maintain the pressure of 15 Pa during the film deposition. The Mg-doped $CuAlO_2$ films were deposited at the substrate temperature of 650 ℃ for 60 min in an ambient with the oxygen partial pressure of 15 Pa. After deposition, all the deposited $CuAl_{1-x}Mg_xO_2$ films were post-annealed in a tube furnace under Ar atmosphere at the temperature of 1000 ℃ for 30 min.

The microstructure, crystal orientation, elementary composition and chemical bonding of the deposited and annealed $CuAl_{1-x}Mg_xO_2$ films were investigated by X-ray diffraction (XRD) and X-ray photoelectron spectroscopy (XPS) with a monochromatized Al Ka X-ray source. The surface morphology of the films was characterized by scanning electron microscopy (SEM). The optical properties of the films were characterized using UV-visible-NIR spectrophotometer. The

electrical properties of the $CuAl_{1-x}Mg_xO_2$ films (x=0, 0.01, 0.02, 0.05) were examined by the four-probe van der Pauw method at room temperature using Hall effect measurement system (Nanometrics HL5500PC). A permanent magnet is applied and the magnetic field strength is 0.5 T.

3. Results and discussion

Figure 1 shows the XRD pattern of sintered $CuAl_{1-x}Mg_xO_2$ (x=0, 0.01, 0.02, 0.05) targets prepared by a conventional solid-state reaction. For the undoped sintered target, all the diffraction peaks of $CuAlO_2$ target without Mg doping can be identified as delafossite structure $CuAlO_2$, and are consistent with the standard JCPDF card (No.75-2361, space group $R\bar{3}m$). No any peaks which belong to the starting materials or impurity phase are observed. The second phase of CuO and $CuAl_2O_4$ can be observed when the Mg dopant is introduced into the sintered targets. However, the MgO phase is not presented in all $CuAl_{1-x}Mg_xO_2$ targets from the XRD patterns. Moreover, with the increase of Mg content, more peaks of impurity phase appear, along with the enhanced intensity of second phase peak. This indicates that the Mg doping results in the decomposition of $CuAlO_2$ phase [32] via the following reaction:

$$4CuAlO_2 + O_2 = 2CuO + 2CuAl_2O_4 \quad (1)$$

The as-deposited $CuAl_{1-x}Mg_xO_2$ films exhibit the amorphous structure at the substrate temperature of 650 ℃. It is well known that the annealing is a very effective method to improve the crystalline of materials. Therefore, the annealing technique is employed for all the as-deposited $CuAl_{1-x}Mg_xO_2$ films by PLD to develop its electrical and optical properties. Figure 2 shows the XRD patterns of the $CuAl_{1-x}Mg_xO_2$ films with various Mg compositions annealed in Ar atmosphere at the temperature of 1000 ℃ for 30 min. The annealing atmosphere of Ar acting as protective atmosphere is applied to avoid the decomposition of $CuAlO_2$ films during the high temperature annealing. It can be seen that the annealed $CuAl_{1-x}Mg_xO_2$ films exhibit

good crystallization and phase-pure. All the peaks are identified to be the reflections of $CuAlO_2$ phase of the delafossite structure without any diffraction peak corresponding to the second phase presented after the annealing treatment, which is different from the XRD patterns of Mg-doped $CuAlO_2$ target. This indicates that the introduction of Mg into $CuAlO_2$ cann't induce the impurity phases after annealing treatment. Meanwhile, the notable peaks corresponding to crystal plane of (003), (006), (009), (104) and (0012) indicate that the $CuAl_{1-x}Mg_xO_2$ (x=0, 0.01, 0.02, 0.05) films are preferentially oriented along the c-axis perpendicular to the substrate surface. This c-axis orientation growth suggests that the surface energy of the (001) family of crystal plane could be the lowest in $CuAlO_2$ crystal. Thus it can be proved that the annealing treatment in Ar atmosphere is beneficial for the formation of pure phase $CuAlO_2$ and (001) orientation growth. However, the intensities of diffraction peaks of $CuAl_{1-x}Mg_xO_2$ films decrease with increasing Mg concentration, meanwhile (0012) peak appears when the Mg concentration increases up to 5 at.%, which reflects the weakened c-axis orientation growth. The decline of the crystalline quality of $CuAl_{1-x}Mg_xO_2$ films may be due to the substitution of Mg^{2+} for Al^{3+}.

As seen in Fig. 2, the (006) peaks for all the $CuAl_{1-x}Mg_xO_2$ (x=0, 0.01, 0.02, 0.05) films shift toward lower angles with the increase of Mg content, which subsequently inferring to the variation of lattice constants *c* shown in Fig. 3. It can be seen that the lattice constant *c* of $CuAl_{1-x}Mg_xO_2$ films gradually increases with increasing the Mg-doping concentration, which reflects the fact of crystal cell expansion. The cell expansion can be ascribed to the substitution of Mg for Al in the $CuAlO_2$ lattice to form substitutional solid solution. Due to the mismatch between the ionic radii, the substitution of Mg^{2+} (0.066nm) ions in Al^{3+} (0.051nm) sites induces lattice distortion, which consequently results in the decline of the crystalline quality.

To further identify the chemical compositions and valences of the elements, XPS analysis was performed to characterize the annealed $CuAl_{1-x}Mg_xO_2$ (x=0, 0.01, 0.02, 0.05) films. Figure 4 shows the XPS wide survey spectra of $CuAl_{1-x}Mg_xO_2$ (x=0, 0.01, 0.02, 0.05) films annealed in

Ar atmosphere at the temperature of 1000 ℃ for 30 min. It can be observed that the spectrum of the undoped $CuAlO_2$ is dominated by C1s, O1s, Cu2p and Al2p peak. The carbon signal perhaps originates from the XPS measurement system. For all the Mg doped $CuAlO_2$ films, the Mg2s signal in the XPS spectra appears, indicating that Mg is successfully doped into the $CuAlO_2$ films. High-resolution XPS scans were acquired for the O1s, Cu2p, Al2p and Mg2s regions of the $CuAl_{1-x}Mg_xO_2$ films with x =5%, as shown in Fig. 5. Figure 5(a) shows the Cu2p core spectrum with the binding energy of $Cu2p_{3/2}$ at about 931.8 eV and $Cu2p_{1/2}$ at about 950.9 eV. There is no shake-up line of $Cu2p_{3/2}$ between peak of $Cu2p_{3/2}$ and $Cu2p_{3/1}$ in the spectrum. The absence of shake-up implies that the valence state of Cu in $CuAl_{0.95}Mg_{0.05}O_2$ film is Cu^+. It is well established that the core level spectrum of Cu^{2+} compounds has a strong shake-up satellite feature which is absent in the core level spectra of Cu^+ compounds [33]. This feature has been widely used for the identification of different oxidation states of copper in various copper compounds. The absence of satellite peaks suggests that valence state of Cu in $CuAl_{0.95}Mg_{0.05}O_2$ film is Cu^+. This is confirmed in other samples with various Mg doping concentrations as well, which suggests that impurity phases of CuO and $CuAl_2O_4$ can be eliminated after annealing treatment. XPS studies along with XRD results indicate that there is only $CuAlO_2$ phase in our samples. Based on the integral intensity of O1s, Cu2p, Al2p and Mg2s peaks, and the intrinsic sensitivity factors of oxygen, copper, aluminum and magnesium, the actual Mg doping contents are calculated to be 0.96%, 1.83%, 4.86% for the film $CuAl_{0.99}Mg_{0.01}O_2$, $CuAl_{0.98}Mg_{0.02}O_2$ and $CuAl_{0.95}Mg_{0.05}O_2$, respectively.

Figure 6 shows the surface morphologies of the obtained $CuAl_{1-x}Mg_xO_2$ films with various Mg doping concentrations annealed in Ar atmosphere at the temperature of 1000 ℃ for 30 min. For the deposition without Mg doping, the undoped $CuAlO_2$ film exhibits continuous, dense and granular structure morphology without obvious micro-cracks. The surface of films is relatively smooth, and the grain size is homogeneous. Then the surface pattern varies with the introduction

of Mg into the $CuAlO_2$ film. With the increase of Mg doping concentration, the particles grow up gradually. Compared to the undoped $CuAlO_2$ film, the $CuAl_{0.95}Mg_{0.05}O_2$ film surface has an obviously larger grain except for some micro-holes, which suggests the decrease of grain boundaries.

The Hall effect measurement is carried out to characterize the electrical properties of $CuAl_{1-x}Mg_xO_2$ films (x=0, 0.01, 0.02, 0.05) at room temperature using the van der Pauw method [34]. The Hall coefficients derived from the Hall measurement for $CuAl_{1-x}Mg_xO_2$ films with x = 0%, 1%, 2% and 5% are 40.76, 14.6, 6.82 and 5.02 m^3/C, respectively. The positive Hall coefficient measured for these films verifies the p-type conduction behavior, indicating that the obtained $CuAl_{1-x}Mg_xO_2$ films are p-type semiconductor. Figure 7 shows the variation of electrical performance parameters (carrier concentration, mobility, and resistivity) of $CuAl_{1-x}Mg_xO_2$ films with the increase of Mg doping concentration. The Hall effect measurement reveals the carrier concentration to be 2.70×10^{17}, 7.71×10^{17}, 1.69×10^{18} and 2.21×10^{18} cm^{-3} for $CuAl_{1-x}Mg_xO_2$ films with x = 0%, 1%, 2% and 5%, respectively. The increase of Mg doping concentration results in carrier concentration increasing, as shown in Fig.7 (a). The p-type conductivity in Cu^+-based delafossites is dominated by d-orbital in $Cu^+(3d^{10})$ with charge compensation of the $Cu^{2+}(3d^9)$. Bivalent cations, such as Mg^{2+}, Ca^{2+}, and Zn^{2+}, doped onto Al^{3+} sites in $CuAlO_2$ with layered structure semiconductor can increase p-type conductivity mainly by contributing to the hole concentration [35, 36]. In the Mg-doped $CuAlO_2$ films, more holes can be formed by a charge-compensating mechanism when Mg^{2+} substitutes for Al^{3+}, which in turn results in the enhancement of p-type conduction. This has been verified in delafossite structure by many reports, such as Mg doped $CuCrO_2$ [37] and Mg-doped $CuFeO_2$ [38].

In addition to the hole carrier concentration, Hall mobility is another significant factor that influences conductivity. By contrast, the Hall mobility decreases from 8.14 to 0.78 cm^2/V s as Mg concentration increases from 0 to 5%, as shown in Fig.7 (b). The results can be attributed to

the weakened c-axis orientation growth and the effect of the grain boundary scattering. According to the XRD results shown in Fig.2, Mg doping is harmful to the preferred c-axis orientation of the $CuAlO_2$ film. Consequentially the lowest Hall mobility of 0.78 cm^2/V s is obtained when the Mg content is further increased to 5%. The film conductivity is determined by the product of carrier mobility and carrier concentration. Combining the measured carrier mobility and carrier concentration, the resistivity of the film is obtained, as shown in Fig.7 (c). It can be clearly seen that the average resistivity of the $CuAl_{1-x}Mg_xO_2$ films decreases from 16.67 to 11.45 Ω·cm as Mg concentration increases from 0 to 2%, and then increases to 20.87 Ω·cm when Mg concentration further increases to 5%. The highest conductivity is obtained for the $CuAl_{1-x}Mg_xO_2$ films with x =2%, which is similar to the reported results for the $CuAl_{1-x}Mg_xO_2$ films deposited by RF magnetron sputtering [23]. The increase of resistivity for the $CuAl_{1-x}Mg_xO_2$ films with x=5% is a result of the increase of the carrier concentration and the decrease of mobility, and is mainly attribute to the lowest Hall mobility of 0.78 cm^2/V s. Moreover, the deposited amorphous $CuAl_{1-x}Mg_xO_2$ films before annealing were highly resistant and their electrical properties were not able to be characterized by the Hall effect measurement. Those results demonstrate that the combination of annealing technique and Mg doping is advantageous for enhancing the electrical conduction of $CuAlO_2$ film.

The optical transmission spectra of $CuAl_{1-x}Mg_xO_2$ (x=0, 0.01, 0.02, 0.05) films are investigated by UV-VIS spectrophotometer. Figure 8 shows the optical transmittance of the obtained $CuAl_{1-x}Mg_xO_2$ films in the range of 200-800 nm. As can be seen, the absorption edges for all the films can be clearly observed and the transmittance of Mg-doped $CuAlO_2$ films decreases with the increment of Mg doping concentration. Compared with the Mg-doped $CuAlO_2$ films, the undoped $CuAlO_2$ film exhibits a relatively high transparence of over 85% in the visible light range. For the $CuAl_{1-x}Mg_xO_2$ film with x=5%, the transmittance decreases to be about 45%. The optical transmittance gradually reduces with the increase of Mg concentration.

The carrier concentration increases and carrier mobility decreases with the increase of Mg concentration in Mg-doped $CuAlO_2$ films, as demonstrated in Fig.7. Increasing carrier concentration and decreasing carrier mobility result in the enhancement of absorption of incident photons [39, 40]. The scattering and absorption of photons in the film resulting from doping lead to the reduction of the optical transmittance [41].

The optical band gap of the annealed $CuAl_{1-x}Mg_xO_2$ (x=0, 0.01, 0.02, 0.05) films can be deduced by Tauc's relation expresses as $(\alpha h\nu)^2=C(h\nu-E_g)$ [42] where C is a constant that depends on the electron-hole mobility, $h\nu$ is the incident photon energy, E_g is the optical band gap, and α is the absorption coefficient, which is obtained near the absorption edge from the transmittance. The graph of $(\alpha h\nu)^2$ vs. hν is plotted to estimate the optical band gap of $CuAl_{1-x}Mg_xO_2$ films, as shown in Fig. 9. By extrapolating the straight portion of the curve, the direct optical band gap is estimated to be 3.54, 3.52, 3.49 and 3.43 eV for the sample of $CuAl_{1-x}Mg_xO_2$ films with x=0, 1%, 2% and 5%, respectively. It is obvious that the E_g of $CuAl_{1-x}Mg_xO_2$ films decreases with increasing the Mg doping concentration, which is in good agreement with the similar results reported by Bhandari [43]. The distortion of the CuO_4 tetrahedra is increased after introducing Mg^{2+} into the lattice, which can cause the dispersion at VBM (valence-band maximum). Therefore, the 3d symmetry of Cu is degraded from D_{2d} into a less symmetrical condition, causing less degenerate Cu 3d states, which makes the VBM increase slightly, consequently resulting in a narrower band gap [44]. Beyond that, the increase of impurities and defects with increasing Mg doping concentration will generate the impurity energy levels, which effectively reduces the optical band gaps of Mg doped $CuAlO_2$ films [23, 45].

4. Conclusions

Single-phase high conductivity transparent p-type delafossite Mg doped $CuAlO_2$ films were successfully deposited on sapphire and fused silica substrates by pulsed laser deposition

followed by annealing at temperature of 1000 ℃ in Ar ambient. The dependence of structural, morphological, electrical and optical properties on Mg doping concentration was found. X-ray diffraction results reveal that the annealed $CuAl_{1-x}Mg_xO_2$ (x=0, 0.01, 0.02, 0.05) films exhibit c-axis orientation without detected secondary phase, and that Mg substitution on Al sites results in lattice distortion and decline of the crystalline quality. The hole concentration increases from 2.70×10^{17} to 2.21×10^{18} cm^{-3} and Hall mobility decreases from 40.76 to 5.02 m^3/C for the $CuAl_{1-x}Mg_xO_2$ films as the Mg doping concentration increases from 0 to 5%. The optimum Mg doping concentration of 2% is achieved with the minimum resistivity of 11.45 Ω·cm at room temperature. With the increase of Mg doping concentration, the optical transmittance is gradually reduced, and the optical band gaps of $CuAl_{1-x}Mg_xO_2$ films are found to decrease from 3.54 to 3.43 eV. Those results demonstrate that the combination of annealing technique and Mg doping is advantageous for enhancing the electrical conduction of $CuAlO_2$ film.

Acknowledgement

This work was financially supported by the Natural Science Foundation of Jiangsu Province of China (BK20141401), the Fundamental Research Funds for the Central Universities (No. 30920130111019, 30920130111017), the State Key Project of Fundamental Research of China (2014CB931702), National Nature Science Foundation of China (61222403).

References

1 T. Earmme, Y.J. Hwang, N.M. Murari, S. Subramaniyan and S.A. Jenekhe, *J. Am. Chem. Soc.*, 2013, 135, 14960-14963.

2 X.H. Zhang, B. Domercq, X.D. Wang, S. Yoo, T. Kondo, Z.L. Wang and B. Kippelen, *Org. Electron.*, 2007, 8, 718-726.

3 Y. Xie, M.G. Gong, T.A. Shastry, J. Lohrman, M.C. Hersam and S.Q. Ren, *Adv. Mater.*, 2013, 25, 3433-3437.

4 Y. Yang, Q.L. Huang, A.W. Metz, J. Ni, S. Jin, T.J. Mark, M.E. Madsen, A. Divenere and S.T. Ho, *Adv. Mater.*, 2004, 16, 321-324.

5 D.S. Leem, T.H. Lee and T.Y. Seong, *Solid-State Electron.*, 2007, 51, 793-796.

6 N. Noor and I.P. Parkin, *J. Mater. Chem. C*, 2013, 1, 984-996.

7 J.I. Kim, K.H. Ji, M. Jang, H. Yang, R. Choi and J.K. Jeong, *ACS. Appl. Mater. Inter.*, 2011, 3, 2522-2528.

8 S.H. Yu, W.F. Zhang, L.X. Li, H.L. Dong, D. Xu and Y.X. Jin, *Appl. Surf. Sci.*, 2014, 298, 44-49.

9 H. Kawazoe, M. Yasukawa, H. Hyodo, M. Kurita, H. Yanagi and H. Hosono, *Nature*, 1997, 389, 939-942.

10 J. Ding, Y.M. Sui, W.Y. Fu, H.B. Yang, S.K. Liu, Y. Zeng, W.Y. Zhao, P. Sun, J. Guo, H. Chen and M.H. Li, *Appl. Surf. Sci.*, 2010, 256, 6441-6446.

11 Z.Q. Sun, X.S. Jiang, J.L. Li, G. He and X.P. Song, *J. Alloys Comp.*, 2013, 581, 488-493.

12 Y.J. Lin, J. Luo and H.C. Hung, *Appl. Phys. Lett.*, 2013, 102, 193511.

13 Z.Q. Yao, B. He, L. Zhang, C.Q. Zhuang, T.W. Ng, S.L. Liu, M. Vogel, A. Kumar, W.J. Zhang and C.S. Lee, *Appl. Phys. Lett.*, 2012, 100, 062102.

14 J. Tate, H.L. Ju, J.C. Moon, A. Zakutayev, A.P. Richard, J. Russell and D.H. McIntyre, *Phys. Rev. B*, 2009, 80, 165206.

15 C. Ghosh, S. Popuri, T. Mahesh and K. Chattopadhyay, *J. Sol-Gel. Sci. Technol.*, 2009, 52, 75-81.

16 Z. Lockman, L. Lin and C.K. Yew, *Sol. Energ. Mat. Sol. C*, 2009, 93, 1383-1387.

17 W. Lan, W.L. Cao, M. Zhang, X.Q. Liu, Y.Y. Wang, E.Q. Xie and H. Yan, *J. Mater. Sci.*, 2009, 44, 1594-1599.

18 R. Nagarajan, A. D. Draeseke, A.W. Sleight and J. Tate, *J. Appl. Phys.*, 2001, 89, 8022.

19 A.C. Rastogi, S.H. Lim and S.B. Desu, *J. Appl. Phys.*, 2008, 104, 023712.

20 D. Li, X. Fang, W. Dong, Z. Deng, R. Tao, S. Zhou, J. Wang, T. Wang, Y.Zhao and X. Zhu, *J. Phys. D : Appl. Phys.*, 2009, 42, 055009.

21 G.B. Dong, M. Zhang, X. Zhao, H. Yan, C. Tian and Y. Ren, *Appl. Surf. Sci.*, 2010, 256, 4121-4124.

22 H.F. Jiang, X.B. Zhu, H.C. Lei, G. Li, Z.R. Yang, W.H. Song, J.M. Dai, Y.P. Sun and Y.K. Fu, *J. Alloys Comp.*, 2011, 509, 1768-1773.

23 G.B. Dong, M. Zhang, W. Lan, P.M. Dong and H. Yan, *Vacuum*, 2008, 82, 1321-1324.

24 Z.H. Deng, X.D. Fang, R.H. Tao, W.W. Dong, D. Li and X.B. Zhu, *J. Alloys Comp.*, 2008, 466, 408-411.

25 H. Gong, Y. Wang and Y. Luo, *Appl. Phys. Lett.*, 2000, 76, 3959.

26 D.S. Kim, S.J. Park, E.K. Jeong, H.K. Lee and S.Y. Choi, *Thin Solid Films*, 2007, 515, 5103.

27 M. Fang, H.P. He, B. Lu, W.G. Zhang, B.H. Zhao, Z.Z. Ye and J.Y. Huang, *Appl. Surf. Sci.*, 2011, 257, 8330-8333.

28 Y.J. Zhang, Z.T. Liu, D.Y. Zang and L.P. Feng, *Vacuum*, 2014, 99, 160-165.

29 R.S. Yu and H.S. Yin, *Thin Solid Films*, 2012, 526, 103-108.

30 J.Q. Pan, S.K. Guo, X. Zhang, B.X. Feng and W. Lan, *Mater. Lett.*, 2013, 96, 31-33.

31 C. Bouzidi, H. Bouzouita, A. Timoumi and B. Rezig, *Mater. Sci. Eng. B*, 2005, 118, 259.

32 B. Yang, Y.M. Lu, C. Neumann, A. Polity, C.Z. Wang and B.K. Meyer, *Mater. Res. Soc.*, 2006, 905, 2-7.

33 B. Balamurugan, B.R. Mehta, D.K. Avasthi, F. Singh, A.K. Arora, M. Rajalakshmi, G. Raghavan, A.K. Tyagi and S.M. Shivaprasad, *J. Appl. Phys.*, 2002, 92, 3304.

34 L.J. van der Pauw, *Philips Res. Rep.*, 1958, 13, 1-9.

35 G.B. Dong, M. Zhang, T.X. Li and H. Yan, *J. Electrochem. Soc.*, 2010, 157, H127- H130.

36 P.M. Dong, M. Zhang, G.B. Dong, X.P. Zhao and H. Yan, *J. Electrochem. Soc.*, 2008, 155, H319-H322.

37 T. Chiu, S.W. Tsai and Y.P. Wang, *Ceram. Int.*, 2012, 38, 673-676.

38 Z.H. Deng, X.D. Fang and S.Z. Wu, *J. Alloys Comp.*, 2013, 577, 658-662.

39 R.A. Smith, Semiconductors, New York: Cambridge, 1961, 216-222.

40 D.K. Schroder, R.N. Thomas and J.C. Swartz, *IEEE J. Solid-St. Circ.*, 1978, 13, 180-187.

41 Y. Ren, G.Y. Zhao and Y.Q. Chen, *Appl. Surf. Sci.*, 2011, 258, 914-918.

42 J. Tauc, R.G. Rovici and A. Vancu, *Phys. Status Solidi.*, 1966, 15, 627-637.

43 R.K. Bhandari, Y. Hashimoto and K. Ito, *Jpn. J. Appl. Phys.*, 2004, 43, 6890.

44 M.L. Liu, F.Q. Huang and L.D. Chen, *Scripta. Mater.*, 2008, 58, 1002-1005.

45 J.A. Sans, J.F. Sánchez-Royo, A. Segura, G. Tobias and E. Canadell, *Phys. Rev. B*, 2009, 79, 195105.

Figure captions:

Fig. 1 XRD patterns of Mg-doped $CuAlO_2$ target, (a) $CuAlO_2$, (b) $CuAl_{0.99}Mg_{0.01}O_2$, (c) $CuAl_{0.98}Mg_{0.02}O_2$, (d) $CuAl_{0.95}Mg_{0.05}O_2$

Fig. 2 XRD patterns of annealed $CuAl_{1-x}Mg_xO_2$ (x=0, 0.01, 0.02, 0.05) films

Fig. 3 Lattice constant (c) of annealed $CuAl_{1-x}Mg_xO_2$ (x=0, 0.01, 0.02, 0.05) films

Fig. 4 The XPS wide survey spectra of annealed $CuAl_{1-x}Mg_xO_2$ (x=0, 0.01, 0.02, 0.05) films, (a) $CuAlO_2$, (b) $CuAl_{0.99}Mg_{0.01}O_2$, (c) $CuAl_{0.98}Mg_{0.02}O_2$, (d) $CuAl_{0.95}Mg_{0.05}O_2$

Fig. 5 XPS spectra of annealed $CuAl_{0.95}Mg_{0.05}O_2$ film, (a) local fine scanning of Cu, (b) local fine scanning of A12p and Cu3p after fitting, (c) local fine scanning of O1s, (d) local fine scanning of Mg2s

Fig.6 SEM images of the surface morphology of the annealed $CuAl_{1-x}Mg_xO_2$ films, (a) $CuAlO_2$, (b) $CuAl_{0.99}Mg_{0.01}O_2$, (c) $CuAl_{0.98}Mg_{0.02}O_2$, (d) $CuAl_{0.95}Mg_{0.05}O_2$

Fig. 7 Variation of electrical performance parameter of annealed $CuAl_{1-x}Mg_xO_2$ (x=0, 0.01, 0.02, 0.05) films, (a) Carrier concentration, (b) Hall mobility, (c) Electrical resistivity

Fig. 8 The room temperature UV-visible transmittance spectra of the annealed $CuAl_{1-x}Mg_xO_2$ (x=0, 0.01, 0.02, 0.05) films.

Fig. 9 The relationship between $(\alpha hv)^2$ and photo energy (hv) for the annealed $CuAl_{1-x}Mg_xO_2$ (x=0, 0.01, 0.02, 0.05) films.

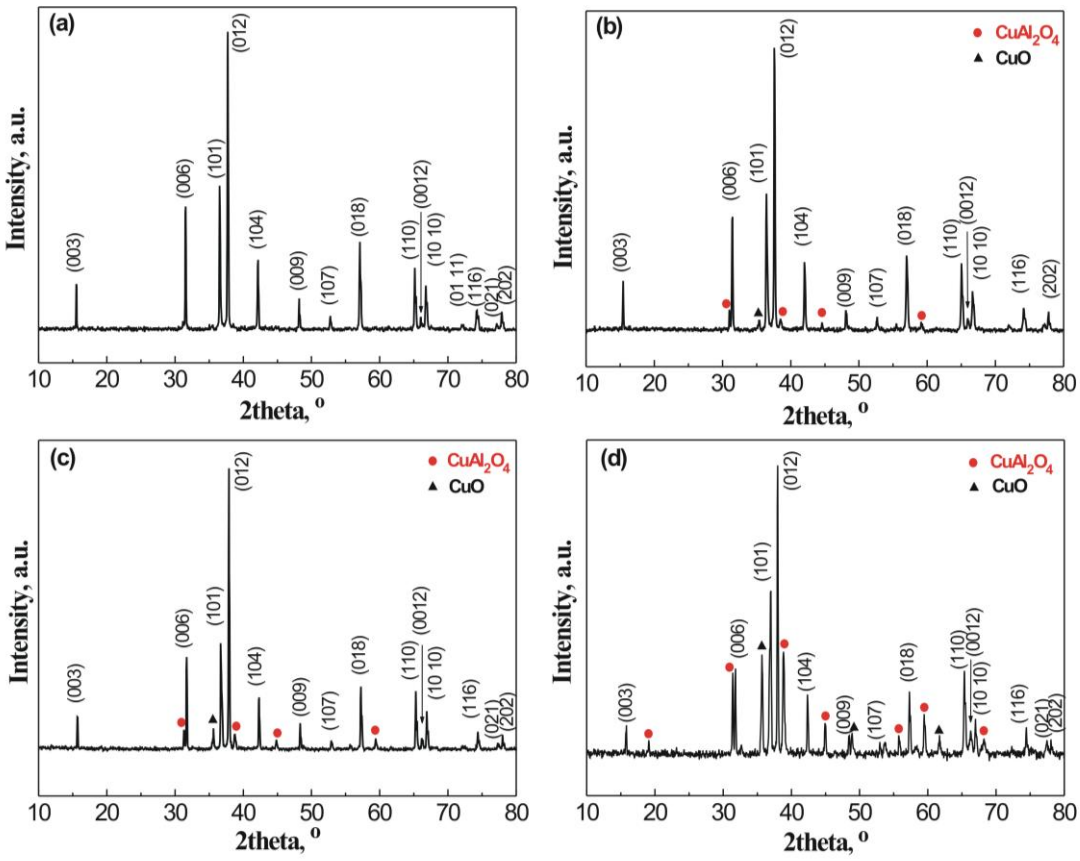

Figure 1

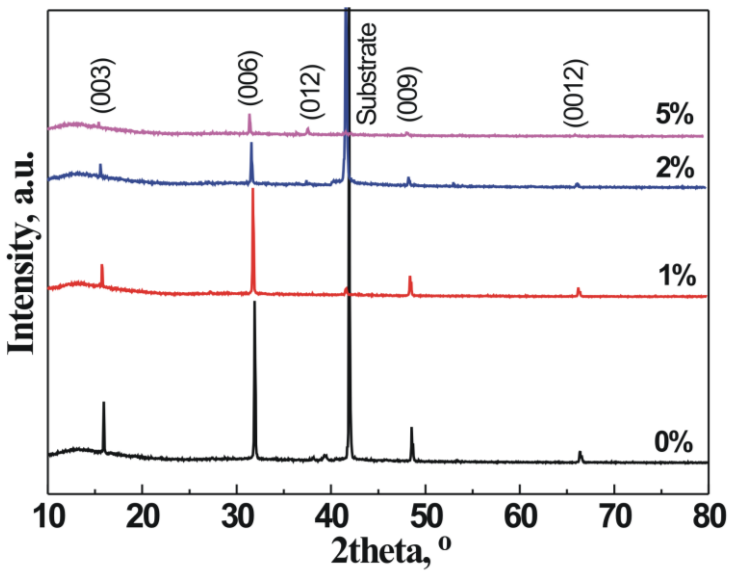

Figure 2

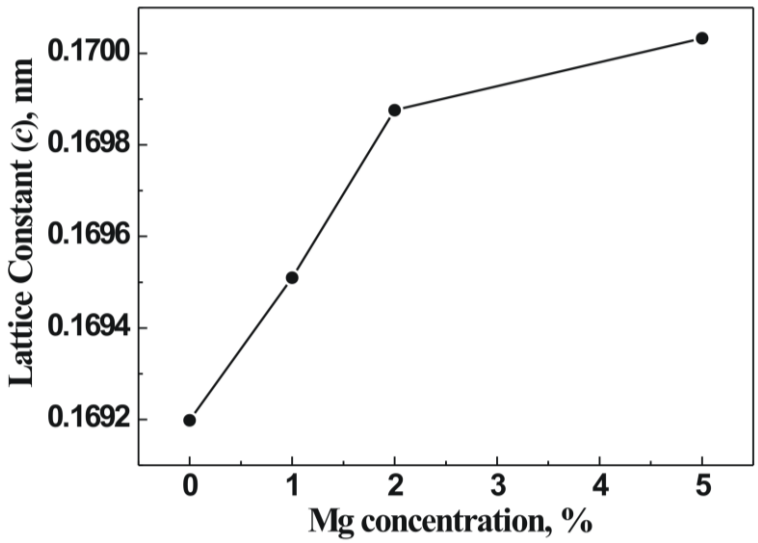

Figure 3

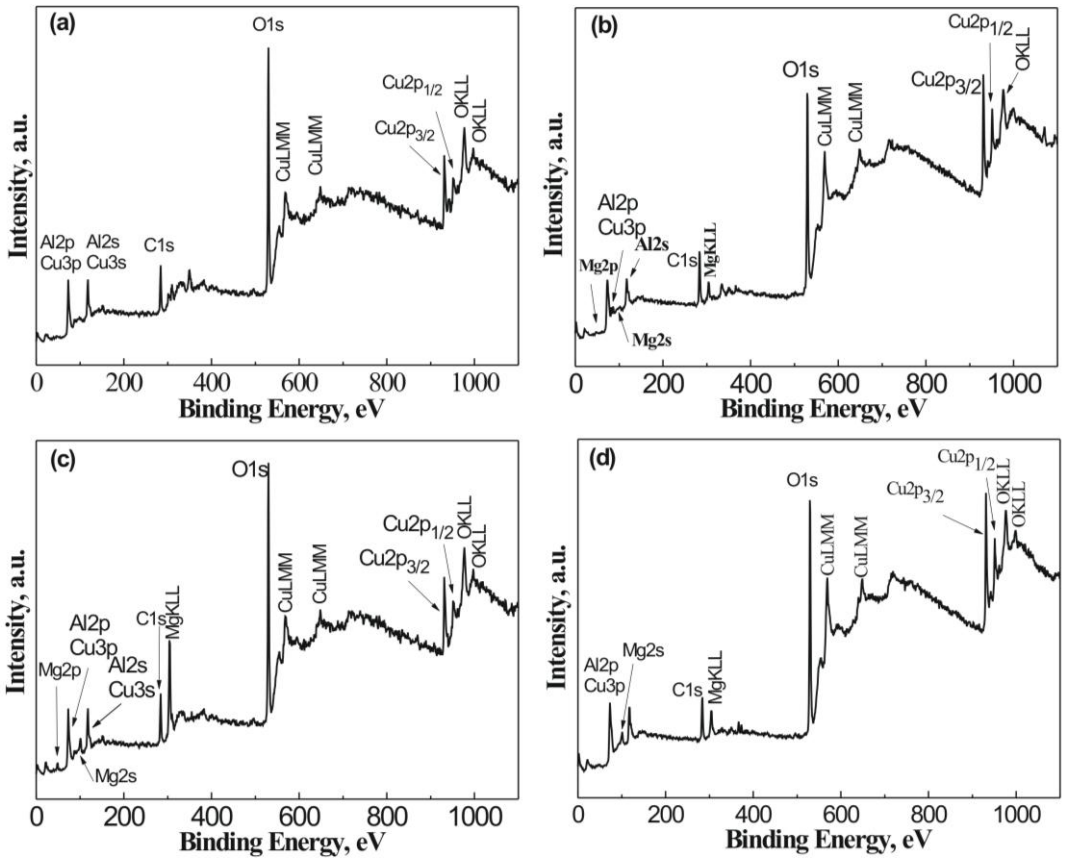

Figure 4

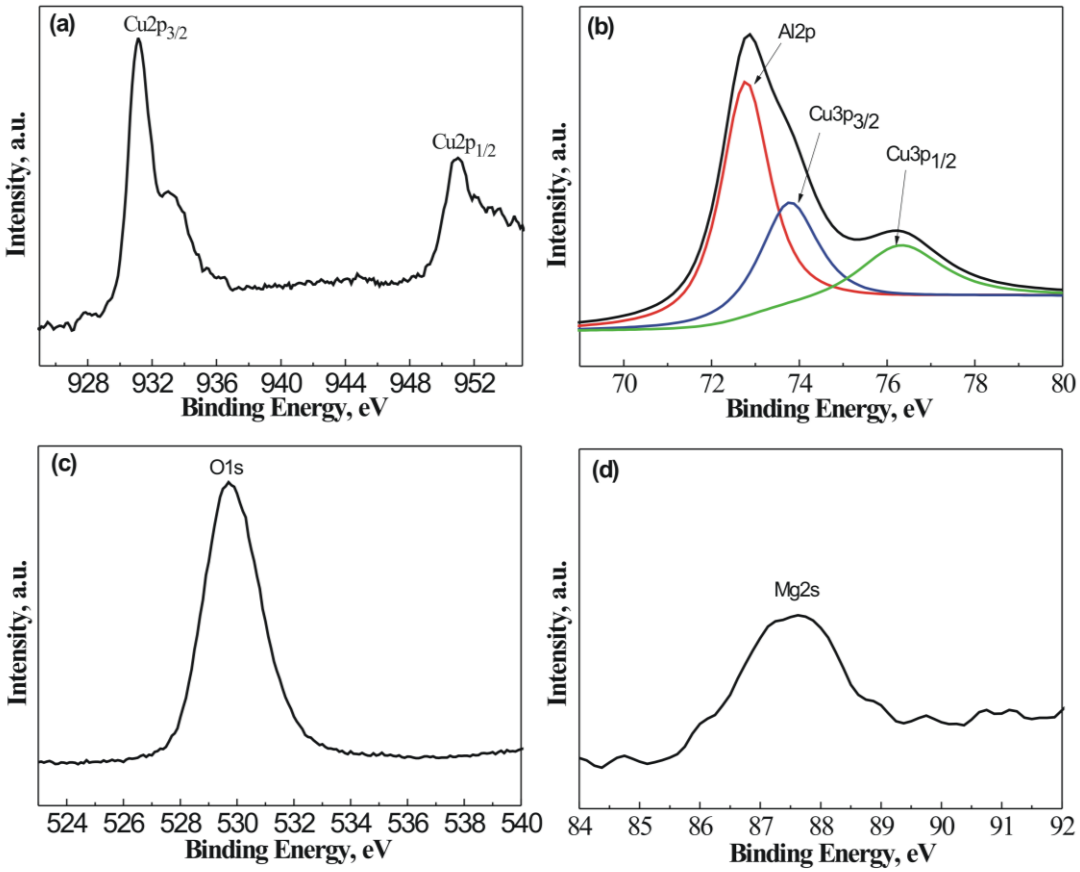

Figure 5

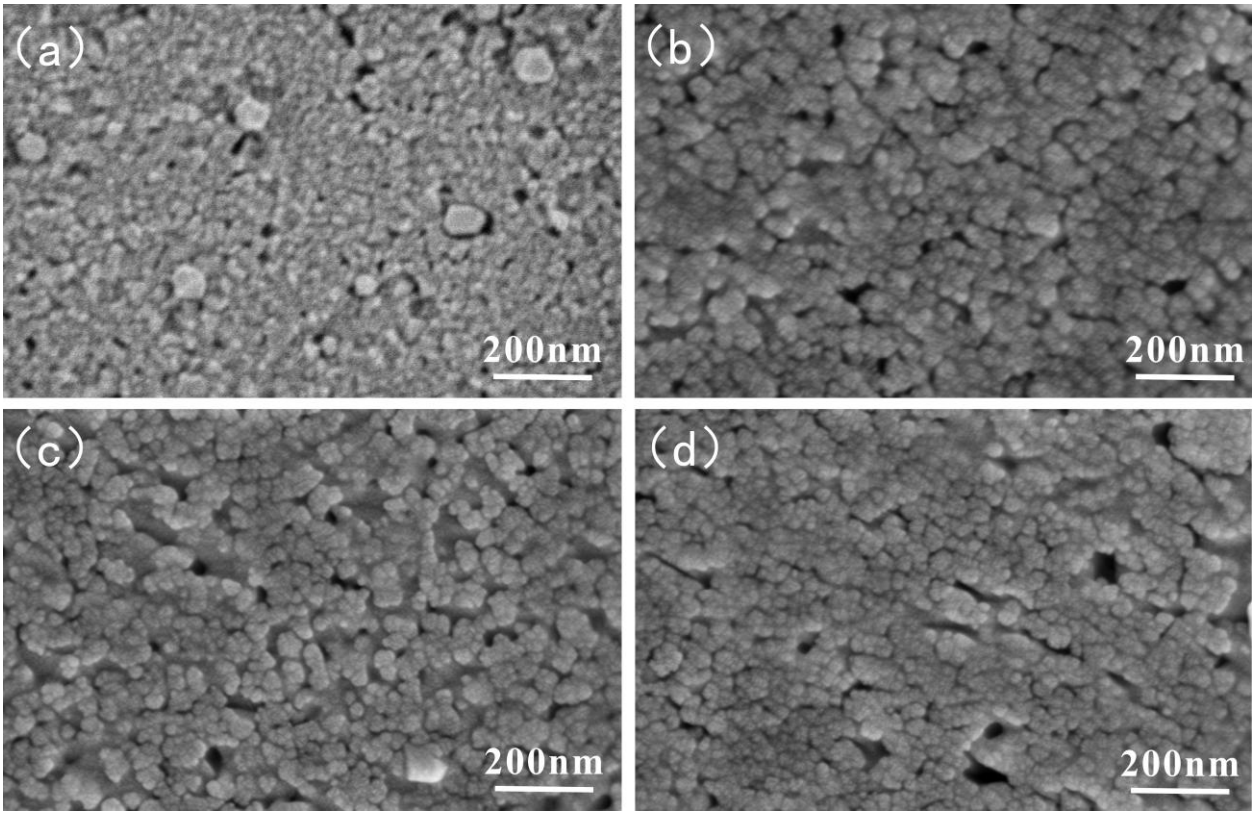

Figure 6

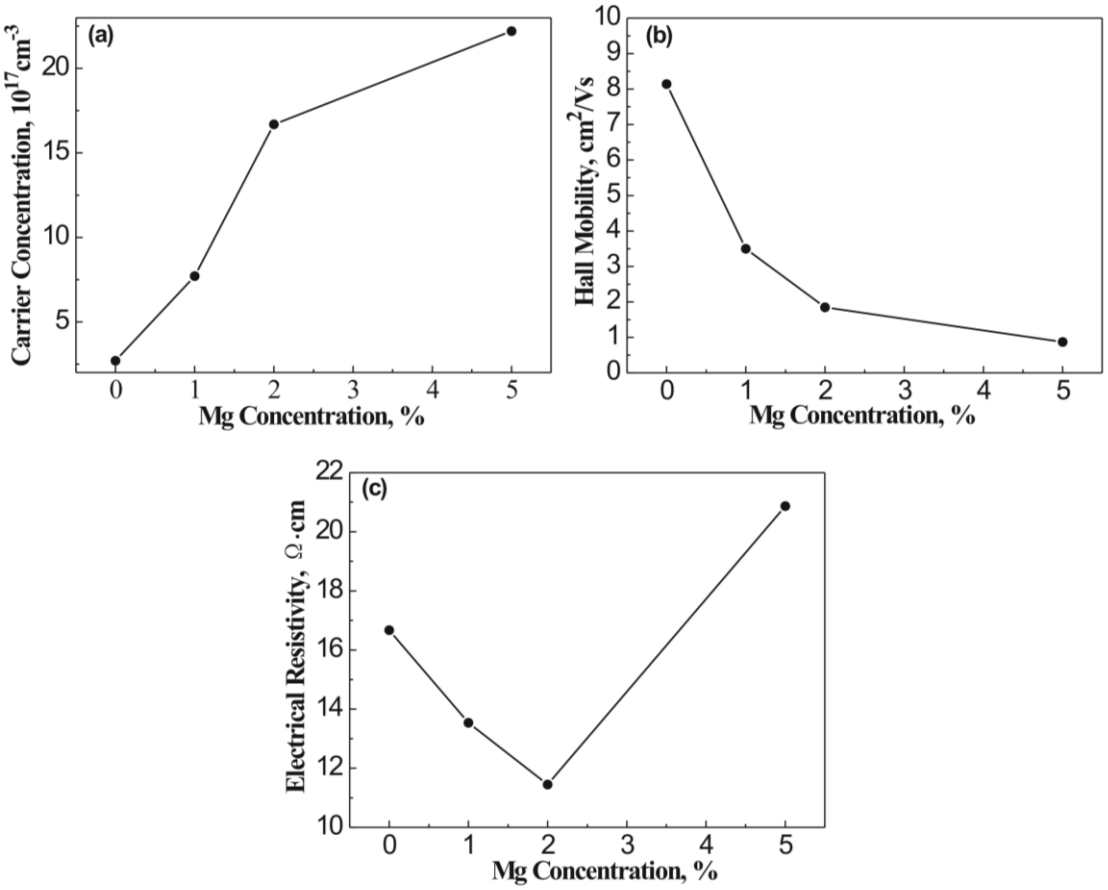

Figure 7

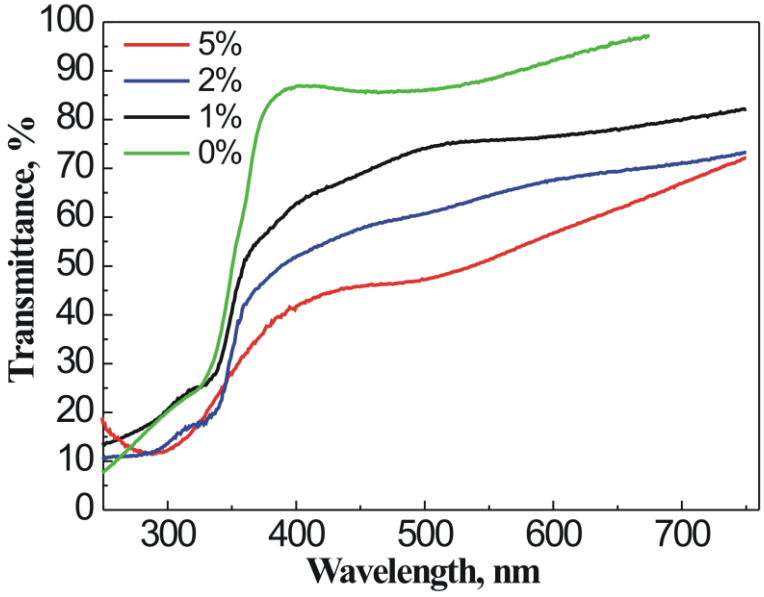

Figure 8

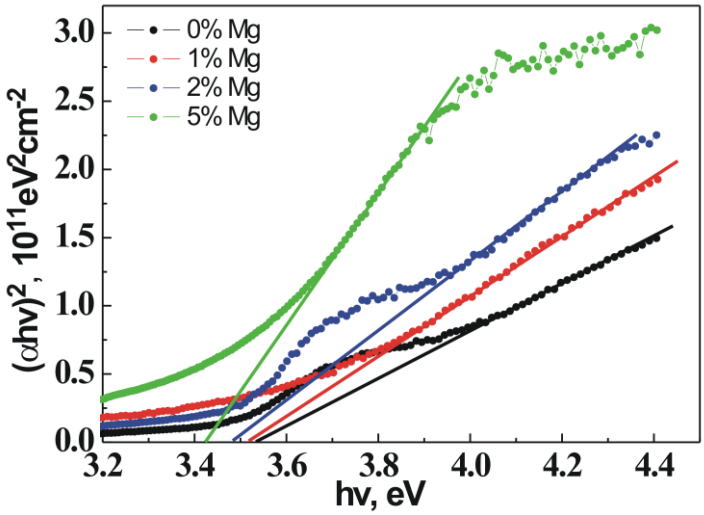

Figure 9